IEEE Access
Multidisciplinary | Rapid Review | Open Access Journal

Received August 9, 2019, accepted September 4, 2019, date of publication September 9, 2019, date of current version September 20, 2019.

Digital Object Identifier 10.1109/ACCESS.2019.2940089

Circularly Polarized Cross-Tapered Bowtie Antenna for IR Polarimetry

SANGJO CHOI[1], (Member, IEEE), AND KAMAL SARABANDI[2], (Fellow, IEEE)
[1]Department of Electrical Engineering, University of Ulsan, Ulsan 44610, South Korea
[2]Radiation Laboratory, Department of Electrical Engineering and Computer Science, The University of Michigan at Ann Arbor, Ann Arbor, MI 48109-2122, USA

Corresponding author: Sangjo Choi (sangjoc@ulsan.ac.kr)

This work was supported by the National Research Foundation of Korea (NRF) grant funded by the Korean Government (MSIT) under Grant 2017R1C1B5076462.

ABSTRACT We propose a novel cross bowtie antenna using phase-shift lines to realize circular polarization (CP) in the infrared (IR) spectrum. The CP antenna consists of a vertical, a horizontal antenna, and two elliptical loops connecting adjacent tips of the antennas to create a 90° phase shift. The phase-shift lines are conceived to realize a single terminal of the antenna where a detecting material can be mounted and enable the detecting material to fully utilize the field enhancement from the antenna. In full-wave simulations, a nanometer-scale low-bandgap semiconductor, i.e., indium gallium arsenide antimonide (InGaAsSb) capable of detecting IR wave is loaded at the antenna terminal and the antenna structure is designed to achieve CP absorption at 180 THz. The antenna includes a transmission line-based impedance matching structure to compensate for the reactance of the InGaAsSb semiconductor load. To verify the CP detection of the antenna near 180 THz, we numerically show a higher field enhancement value and absorption rate in the antenna terminal in a specific CP case when the antenna is illuminated with incident waves with various polarization states. Also, we design 2 × 1 and 2 × 2 antenna arrays using the CP antennas connected with metallic traces and show that the CP absorption at 180 THz is maintained. Finally, an illustration of a focal plane array based on the proposed CP cross bowtie antennas coupled with the InGaAsSb for a full Stokes polarimeter is presented.

INDEX TERMS Infrared antenna, nanoantenna, circularly polarized antenna, stokes vector, infrared full Stokes polarimetry.

I. INTRODUCTION

Imaging polarimetry can measure the polarization state of a field emitted from a scene, as well as the intensity and color that can be detected by traditional infrared (IR) imagers. Polarization information associated with the vector characteristics of light waves can represent the surface roughness, shape, and shading of a target material, which are not related to the intensity or color [1], [2]. Specifically, IR polarimeters are suitable for target identification and use in biomedical imaging as well as material science, for which analysis of the morphology of biological tissues and specimen is required [3]–[5]. The reason is that the IR waves have micron-sized wavelengths and show higher penetration depths in materials than the visible light.

The polarization state of an arbitrarily polarized wave can be represented by the Stokes vector, which is consisted of S_0, S_1, S_2, and S_3. S_0, S_1, and S_2 can be calculated from linearly polarized components of the electric field, but S_3 can be achieved from circularly polarized (CP) components of the electric field [1]. In the visible to IR spectrum, wire grid polarizers are commonly used to transmit a specific linear polarization and this structure was utilized for achieving parts of the Stokes vector (S_0, S_1, and S_2) [6]–[8]. However, it has been challenging to realize a full Stokes polarimeter which can characterize the fourth element (S_3) of the Stokes vector due to difficulty in achieving a planar-type CP polarizer. A CP polarizer can be made by combining a linear polarizer with quarter-wave plates made up of birefringent crystals. However, this structure requires additional components to the imager and fabrication of the birefringent quarter-wave plates with a nanometer-scale is also challenging [9], [10]. For ease of fabrication, liquid crystal polymers where their polarization can be controlled by using the ultraviolet illumination was introduced [9]. With the liquid crystal polymer, polarizing focal plane arrays were constructed and the arrays were

The associate editor coordinating the review of this manuscript and approving it for publication was Mingchun Tang.

 This work is licensed under a Creative Commons Attribution 4.0 License. For more information, see http://creativecommons.org/licenses/by/4.0/

placed on top of image sensors to form full Stokes imaging polarimeters in the visible to IR range [3], [11]–[15]. Also, engineered birefringent materials such as sub-wavelength dielectrics or metal grating structures have been studied for realizing CP-sensitive devices [10], [16]–[22].

Recently, various antenna elements in the form of cross dipole [23]–[26], double dipole [27], V-, and L-type antennas [28], [29], patch antenna [30], and cross aperture [31] were introduced for converting linearly polarized incident waves into either reflected or transmitted CP waves in the IR range. In Ref. [20], a cross dipole antenna structure was illuminated with a CP wave and the enhanced field near the feed gap was reported [23]. To be used for a polarimeter, this structure requires a separate detector such as a spectrometer or a sensor because the antenna was not integrated with any detector material. The antennas coupled with detecting materials such as bolometers, Schottky diodes, and metal-insulator-metal (MIM) diodes are mainly investigated for CP-blind IR detectors [32]–[37]. Although most of the antenna structures are based on the traditional dipole antenna which is sensitive to linearly polarized waves, CP-sensitive spiral antennas coupled with a bolometer were fabricated and studied in the IR regime [32], [33]. Spiral antennas are broadband; however, their major drawbacks, for the application at hand, are their relatively large dimensions and difficulties in making arrays of them.

In this paper, we introduce a new type of the cross bowtie antenna for CP wave detection in the IR spectrum and its array designs for a focal plane array which can be used for a full Stokes polarimeter. Instead of using four separate antenna arms of the optical cross dipole antenna [23]–[26], the proposed antenna utilizes two elliptical loops which connect adjacent tips of a vertical and a horizontal antenna. The elliptical loops are used to provide a 90° phase shift between vertically and horizontally polarized electric fields for CP operation of the antenna and realize a single terminal of the antenna. Thus, when an active material is placed in the terminal, the field enhancement near the antenna terminal due to the plasmonic effect can be utilized efficiently [34]. Different from the reported cross dipole antennas [23]–[26], the proposed antenna can be fed by a voltage gap source in the single terminal so that the critical parameter for the antenna design in optical frequencies, the antenna input impedance, can be calculated [38], [39].

The metallic antenna in the optical domain is known as a device which can concentrate the incident wave into a sub-wavelength in a nanometer-scale [34]; thus the single terminal is designed to be in such a small scale and this size determines the dimension of active material for IR detection. Throughout this paper, the dimension of the semiconductor material is fixed with 30 nm × 30 nm × 30 nm and one of the low bandgap semiconductors, Indium Gallium Arsenide Antimonide (InGaAsSb) is chosen as a detecting material due to its high quantum efficiency in the IR spectrum [40]. The center of the frequency band for the CP operation of the antenna is chosen with 180 THz, where the maximum quantum efficiency of the InGaAsSb occurs [40].

In the antenna design procedure, a vertically polarized bowtie antenna is presented firstly as a fundamental element of the CP bowtie antenna. Then, we show the geometry of a cross bowtie antenna for CP detection at 180 THz. Here, the antenna structures are not loaded with the InGaAsSb material yet and its loading effect will be considered later. To determine the antenna dimensions for efficient CP wave detection at 180 THz, we calculate the radiated field and the input impedance of the antenna by feeding the antenna (in radiation mode) with a voltage gap source in the terminal and the resonant frequency is determined [38], [39], [41]. This antenna design method rests upon the reciprocity; the designed antenna for CP wave radiation at the desired band (180 THz) is equivalently functional for receiving the CP wave at the same band.

As a final step of the antenna design, the InGaAsSb material is loaded at the single terminal of the cross bowtie antenna to realize an IR CP detector. In full-wave simulations, the antenna load is modeled with dielectric constant and conductivity values of the InGaAsSb from 100 THz to 300 THz [40]. However, one issue is that the loading effect of the InGaAsSb with high dielectric constants (∼16) significantly lowers the resonant frequency of the antenna and perturbs the CP detection at 180 THz. Thus, an antenna impedance matching structure using transmission stub lines is connected to the antenna terminal so that the reactance of the load can be canceled effectively [41]. The overall structure is determined to maintain the CP property of the fields in the load at 180 THz when the antenna is illuminated with two perpendicularly polarized incident waves, separately. For verification of CP detection from the InGaAsSb-coupled cross bowtie antenna, the field enhancement and the absorption rate in the antenna terminal are calculated when the antenna is illuminated with incident waves with various polarization states.

Finally, the InGaAsSb-coupled cross bowtie antennas are configured as antenna arrays where the ends of adjacent bowtie antennas are connected using thin metallic traces. Because the proposed antenna does not require additional sensors due to the integration with the InGaAsSb, an array of the antennas can be directly utilized for a focal plane array of a full Stokes polarimeter. In the simulation, the CP performance and field enhancement value from the single antenna are maintained in the 2 × 1 and 2 × 2 arrays and an illustration of a focal plane array is presented. Also, it is worth to note that this proposed design method for the cross bowtie antenna with CP detection can be applied to any arbitrary semiconductor material and desired optical frequencies.

II. ANTENNA DESIGN PROCEDURE

A. VERTICALLY POLARIZED BOWTIE ANTENNA

As a first step for designing a CP cross bowtie antenna, a vertically polarized bowtie antenna without being loaded with the InGaAsSb block is designed as shown in Fig. 1. The

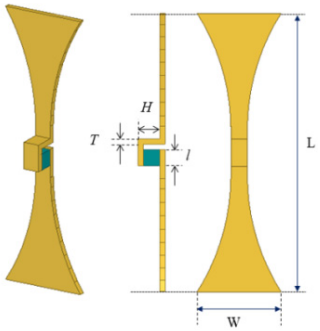

FIGURE 1. Vertically polarized tapered-bowtie antenna geometry loaded with a vacuum block at the terminal.

two bowtie shapes of the antenna are placed at one plane and two arms of the antenna structure are extended such that one of them covers the other arm along the load area with 30 nm × 30 nm. Thus, the overlapped area can accommodate a nanometer-sized semiconductor load and enhanced field from the antenna is applied to the semiconductor efficiently. Similar structures, where silicon dioxide or indium gallium arsenide phosphide (InGaAsP), is sandwiched between two metallic arms of the antenna were reported and fabricated using electron beam lithography [37], [42].

Here, the bowtie antenna is loaded with a void (vacuum) instead of the InGaAsSb load at the terminal because the semiconductor load complicates the antenna design procedure by reducing the resonant frequency of the antenna. All the metallic parts of the antenna structure are modeled by the Drude formula of gold in the IR spectrum [43] and a dimension of a vacuum block loaded at the terminal of the antenna is set to be 30 nm × 30 nm × 30 nm. High-frequency structure simulator (HFSS) using finite element method (FEM) is used for all the modeling and mesh sizes less than 5 nm are used for the antenna structures. The intrinsic input impedance of the bowtie antenna is calculated by de-embedding the capacitance of the vacuum block (30 nm × 30 nm × 30 nm) from the simulated input impedance of the antenna loaded with the vacuum [38], [41]. The input impedance of the antenna is calculated by using a voltage gap source located at the antenna terminal and the capacitance of the vacuum block is achieved from a separate simulation to consider the fringing effect, accurately.

Fig. 1 shows the tapered bowtie antenna with L = 505 nm, W = 150 nm, H = l = 30 nm, and T = 10 nm. Also, the bowtie shape is tapered to prevent antenna performance degradation when the ends of the antenna are connected by thin metallic traces to construct a focal plane array. Fig. 2 shows the input impedance of the vertically polarized tapered-bowtie antenna loaded with the vacuum and the intrinsic input impedance where the capacitance of the vacuum is de-embedded. The solid line for the intrinsic input impedance of the antenna shows the parallel resonance at 180 THz and the resistance is ∼2.84 kΩ. The antenna dimensions which have high resistance at the parallel resonance (180 THz) are chosen to obtain input impedance matching with the high resistive InGaAsSb

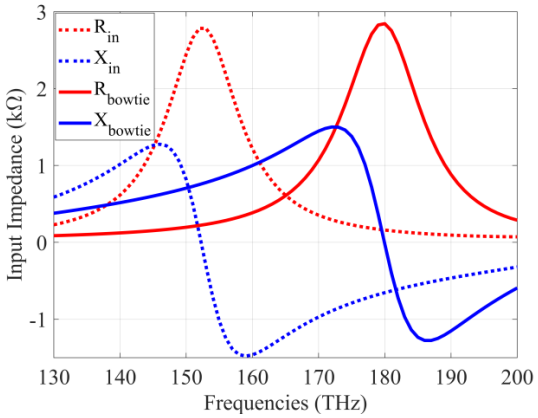

FIGURE 2. Input impedance ($R_{in}+jX_{in}$) of the tapered bowtie antenna loaded with the vacuum and the intrinsic input impedance ($R_{bowtie}+jX_{bowtie}$) of the antenna (the vacuum is de-embedded).

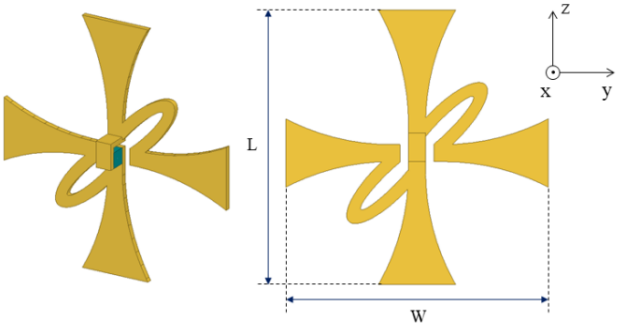

FIGURE 3. CP cross-tapered bowtie antenna structure loaded with the vacuum at the terminal.

block for maximizing power transfer [41]. The high resistance of the InGaAsSb load comes from its low conductivity and small cross section.

B. CIRCULARLY POLARIZED BOWTIE ANTENNA WITH VACUUM LOAD

Based on the vertically polarized bowtie antenna, a cross bowtie antenna loaded with the vacuum for CP radiation at 180 THz is designed as shown in Fig. 3. The cross bowtie antenna consists of a vertical, a horizontal tapered-bowtie antenna and two ellipses for creating 90° phase shift. The ellipses in the first and third quadrants or the second and fourth quadrants generate right-handed CP (RHCP) or left-handed CP (LHCP) radiation in the boresight of the antenna, respectively. Thus, the antenna structure in Fig. 3 is designed for RHCP. To determine the CP operation in the antenna boresight at 180 THz, we load the vacuum at the antenna terminal firstly and tune the lengths of the horizontal bowtie antenna and the ellipses for the phase shift. In the antenna optimization procedure, the radiated electric field in the far-field region is calculated by applying a gap source in the antenna terminal. For accurate calculations of the radiated field components in the far-field, perfectly matched layer (PML) boundary conditions are used.

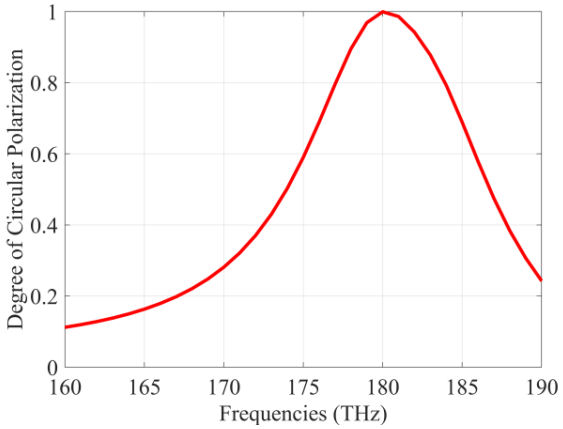

FIGURE 4. The degree of CP in the boresight of the cross-tapered bowtie antenna (L = 480 nm and W = 460 nm) loaded with the vacuum.

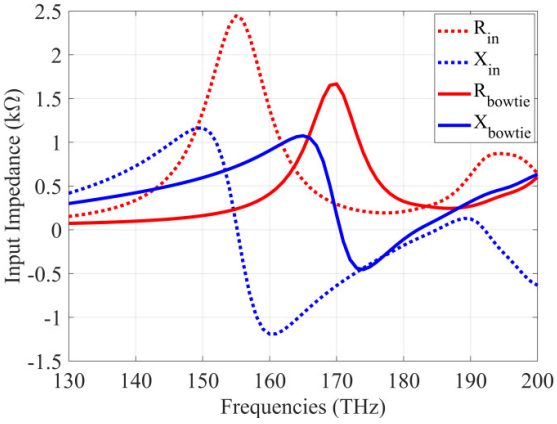

FIGURE 5. Input impedance ($R_{in}+jX_{in}$) of the cross-tapered bowtie antenna loaded with the vacuum and the intrinsic input impedance ($R_{bowtie}+jX_{bowtie}$) of the antenna (the vacuum is de-embedded).

Firstly, 90° phase shift between θ and ϕ components of the radiated electric field (E_θ and E_ϕ) in the boresight is realized when the length of the horizontal bowtie antenna (W) is 460 nm which is shorter than 505 nm of the length of the vertical bowtie (L). This case still does not fulfill the condition for the same magnitude of E_θ and E_ϕ in the boresight. Thus, the vertical bowtie antenna's length (L) is shortened to 480 nm, and then the same magnitude of E_θ and E_ϕ in the boresight is realized. In the optimum design shown in Fig. 3, the length of the horizontal bowtie antenna (W) is maintained as 460 nm, and the major and minor axes of the ellipses are 100 nm and 30 nm, respectively. Fig. 4 shows the degree of CP using $S_3 / I = -2\mathrm{Im}(E_\theta E_\phi^*) / (|E_\theta|^2 + |E_\phi|^2)$ in the boresight of the cross-tapered bowtie antenna loaded with the vacuum after optimization and the perfect CP radiation ($S_3 / I = \sim 1$) is shown at 180 THz.

Also, the input impedance of the cross-tapered bowtie antenna loaded with the vacuum and the intrinsic input impedance of the antenna is simulated and shown in Fig. 5. One thing to note is that the parallel resonance of the intrinsic input impedance of the antenna occurs near 170 THz whereas

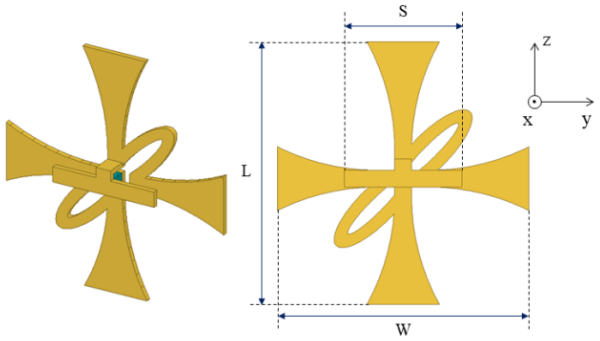

FIGURE 6. CP cross-tapered bowtie antenna structure connected with open-ended transmission lines and loaded with the InGaAsSb block.

the second series resonance occurs near 180 THz. It means that the CP radiation occurs in the series resonance mode instead of the parallel resonance mode. This series resonance mode supports the highest current near the terminal and the ellipses, which can increase the metallic loss from the antenna. In fact, simulations show that the radiation efficiency of the antenna at 180 THz is rather low (value is about 8.5%). Here, the radiation efficiency is calculated with a ratio between the accepted power and the radiated power when the antenna is fed by a voltage gap source. In addition, due to the low resistance of the series resonance at 180 THz, we can expect that the impedance matching between the antenna and the load cannot be realized at the CP radiation mode when the antenna is loaded with the highly resistive InGaAsSb block. This impedance mismatch may cause a lower field enhancement in the terminal at the CP mode compared to that at the parallel resonance mode. To overcome this issue, we will introduce an impedance matching structure in the next chapter.

C. CIRCULARLY POLARIZED BOWTIE ANTENNA WITH InGaAsSb LOAD

As a final step, the cross bowtie antenna is loaded with the InGaAsSb block and its loading effect at the terminal of the antenna is considered. This loading effect complicates the antenna tuning procedure used for achieving the CP property and high field enhancement from the IR antenna because the high capacitance of the InGaAsSb block significantly lowers the resonant frequency of the antenna. Thus, an impedance matching method to compensate for the capacitance of the InGaAsSb load at the resonant frequency should be applied to the CP antenna design procedure. To cancel the high capacitance of the InGaAsSb at 180 THz, we connect two shunt and open-ended inductive transmission lines on the upper plate of the antenna terminal symmetrically, as shown in Fig. 6. Previously, the transmission line structures were used for linearly polarized antennas in the IR spectrum to improve input impedance matching, but the connection to the antenna terminal was not symmetrical [41], [44]. However, the proposed CP antenna should utilize the symmetrical transmission lines not to perturb the CP radiation at 180 THz.

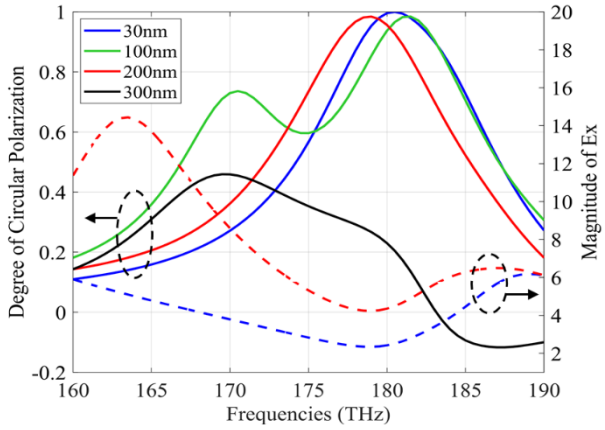

FIGURE 7. The degree of CP in the boresight of the cross-tapered bowtie antenna (L = 480 nm and W = 460 nm) loaded with the InGaAsSb in cases of S = 30 nm, 100 nm, 200 nm, and 300 nm (solid lines) and the magnitude of the × components of the electric field at the center of the InGaAsSb load in the cases of S = 30 nm and 200 nm (dashed lines).

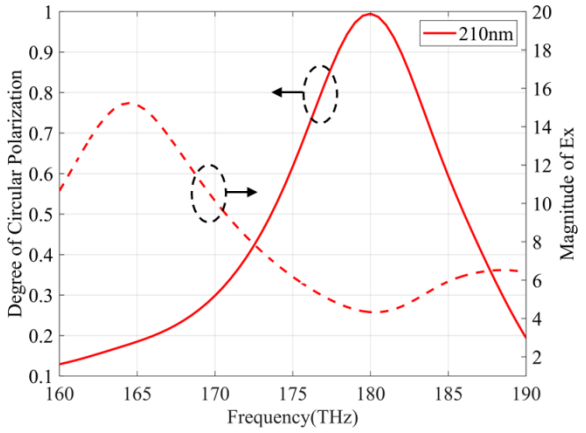

FIGURE 8. The degree of CP in the boresight of the cross-tapered bowtie antenna (L = 470 nm, W = 450 nm, and S = 210 nm) loaded with the InGaAsSb and the magnitude of the × components of the electric field at the center of the InGaAsSb load.

In the simulation, the length of the transmission line stub (S) is varied from 0 nm to 300 nm with a 100 nm step to observe the CP property of the antenna at 180 THz. For the calculation of the degree of CP, the antenna is illuminated with vertically and horizontally polarized plane waves at normal incidence and the electric field components normal to the surface inside the antenna terminal (E_x) for both incident wave polarizations are calculated. For the accurate near-field calculation, mesh sizes less than 3 nm are used inside the InGaAsSb block. Fig. 7 shows the degree of CP values using $S_3/\ I = -2\mathrm{Im}(E_{x(V)}E^*_{x(H)})\ /\ (|E_{x(V)}|^2 + |E_{x(H)}|^2)$ for all the different stub lengths. Here, $E_{x(V)}$ and $E_{x(H)}$ mean the x components of the electric fields at the center of the InGaAsSb load with the vertically and horizontally polarized wave illumination, respectively. Also, the magnitude of the E_x for S = 30 nm and 200 nm for the vertical polarization incidence is included in Fig. 7. Here, the method using the induced fields in the load for determining the CP property of the antenna in the optical regime is a correct way, which is different from a method that uses the scattered field in the far-field region when the antenna is illuminated by only one linearly polarized incident wave [27]. The reason is that scattered field from the nanoantenna structure can distort its polarization property which should be determined using the radiated field obtained from reflection due to load mismatch.

From Fig. 7, we can observe that without the transmission line stub (S = 30 nm), the degree of CP is near unity at 180 THz, but the field magnitude is lower than the value for S = 200 nm. The lower field magnitude for S = 30 nm case is due to the impedance mismatch between the antenna and the InGaAsSb block. In the case of S = 200 nm, the field enhancement value is higher than the value for S = 30 nm and the degree of CP is unity near 180 THz. Thus, we expect that the perfect CP and high field enhancement can be simultaneously achieved when S is near 200 nm. Based on this length for S, the dimensions (L, W) of the vertical and horizontal bowtie antennas and the length of the transmission lines (S) are tuned slightly for the perfect CP and high field enhancement at 180 THz. Finally, when the dimensions of the antenna are S = 210 nm, L = 470 nm, and W = 450 nm, almost perfect CP feature (S_3 / I = ∼0.99) and a high field enhancement value (E_x =∼4.5) at 180 THz are achieved as shown in Fig. 8. The high field magnitude is realized by canceling the capacitance of the InGaAsSb with the inductance of the transmission line stub connected to the antenna terminal at 180 THz [41]. The final dimensions for Fig. 8 should be correct for the perfect CP detection at 180 THz, which are different from those obtained using the method described in [45] because the CP antenna presented in [45] is designed based on the scattered field. In addition, the fractional bandwidth with the degree of CP larger than 0.5 is 6.94%. This bandwidth, which is wider than 6.2 % from the similar antenna topology operating at 2.58 GHz, results from a low Q factor due to the high metallic loss in the IR range [46].

III. FIELD ENHANCEMENT AND ABSORPTION RATE

For verification of the sensitivity of the cross bowtie antenna structure from the incident CP radiation, the field enhancements in the terminal of the antenna for different polarization states (e.g., vertically polarized, RHCP, and LHCP) of the incident wave are simulated as shown in Fig. 9. Here, the field enhancement is defined as the total electric field intensity in the center of the InGaAsSb load divided by the intensity of the incident wave (1 V/m). Because the antenna has the ellipses in the first and third quadrants, we expect that the highest field enhancement from RHCP radiation at 180 THz. In the simulation, when the RHCP wave impinges on the antenna at normal incidence, a highest field enhancement factor of 6.5 is achieved compared to the values of 0.7 and 4.4 for the LHCP and vertical polarization cases at 180 THz. In addition, the absorption rate, defined as a ratio between the power delivered to the InGaAsSb block and the accepted power to

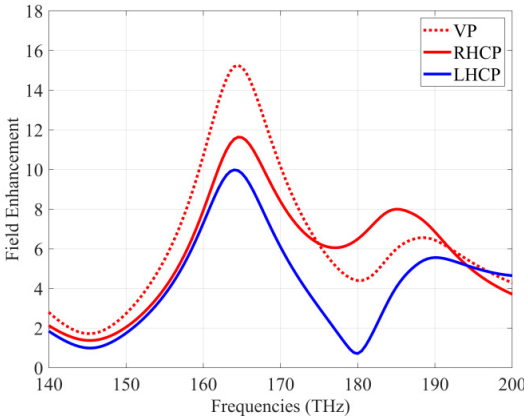

FIGURE 9. The field enhancement in the InGaAsSb block of the cross-tapered bowtie antenna for different polarization states of the incident wave (vertical polarization, RHCP, and LHCP).

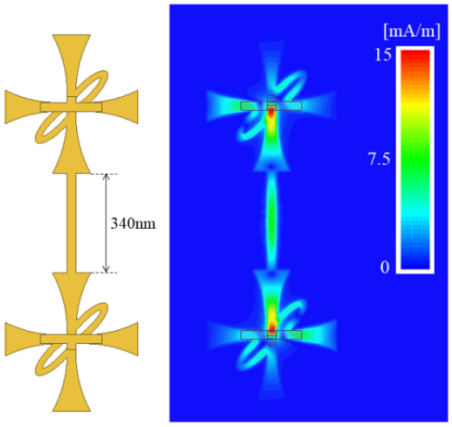

FIGURE 10. The geometry of the 2 × 1 cross bowtie antenna array and surface current distribution (tangential magnetic field) on the surface of the antennas with the vertically polarized wave illumination.

the antenna, is calculated depending on the polarization states of the incident waves. Compared to 3.71% absorption rate at 180 THz for the vertical polarization case, a significantly higher absorption rate of 25.88% is achieved for the RHCP case, which is much higher than the efficiencies (8.58% $\sim$ 13.7%) from a spiral-shaped structure which guides the CP incident wave to a central aperture [16]. These results demonstrate that the designed cross-tapered bowtie antenna coupled with the InGaAsSb is capable of efficiently sensing the RHCP feature of the incident wave near 180 THz.

In Fig. 9, it should be also noted that the maximum field enhancement occurs at $\sim$165 THz for all polarization states of the incident wave. This phenomenon is due to the high input resistance of the cross bowtie antenna near 165 THz and this frequency is similar to the parallel resonant frequency of the intrinsic input impedance of the vacuum-loaded antenna shown in Fig. 3. This finding indicates that the intrinsic resonance of the antenna is maintained even if the InGaAsSb block is loaded and confirms that the capacitance of the InGaAsSb block is effectively compensated for by the inductance of the open-ended transmission lines.

Another interpretation from Fig. 9 is that the field enhancement at 180 THz, where the CP absorption occurs, is lower than the value at 165 THz. This mismatch between frequencies for the CP radiation/absorption and the maximum field enhancement was observed in another CP cross dipole antenna operating in the IR spectrum [24]. By analyzing the intrinsic input impedance of the antenna calculated from the voltage gap source, we can understand that this discrepancy is caused by the resonance mode difference of the CP antenna. That is, the series and parallel resonance are related to the CP radiation/absorption and the maximum field enhancement, respectively. The current distribution required for CP radiation/absorption corresponds to a series resonance which supports the maximum displacement current in the antenna load. However, the maximum field intensity is attributed to the high resistance nature of the parallel resonance of the antenna. Although the highest field enhancement does not occur at the CP operation frequency, the InGaAsSb-coupled cross bowtie antenna can be used to construct a focal plane array for polarimetry because it is capable of achieving a higher field enhancement value and absorption rate in response to a particular CP incident wave near 180 THz.

IV. FOCAL PLANE ARRAY FOR POLARIMETRY

To utilize the CP cross bowtie antenna coupled with the InGaAsSb for IR polarimetry, we design the antenna array structures and use metallic traces for interconnection. For detector applications, metallic traces should be connected to the antennas in the array to collect the current generated by each antenna's load when IR incident waves are illuminated. A method of constructing the antenna array for a bolometer-based IR detector was realized by connecting metallic traces to the ends of the bowtie antennas [47]. In the structure reported in [47], the lengths of the metallic traces were not varied to reduce interference between antenna elements. In this study, two antenna array structures are designed in a similar way using metallic traces and the trace lengths are optimized not to disturb the current distribution of each antenna element. To be used as an IR polarimeter, the antenna array should maintain the CP detection capability at the desired band. Therefore, the antenna array is designed to satisfy the unity degree of CP at 180 THz by adjusting the lengths of the metal traces. In addition, by calculating the surface current distribution of the antennas and the metallic traces and the field enhancement of each antenna element with the vertically polarized wave illumination, we demonstrate that each antenna in the antenna arrays does not interfere with each other and maintains the performance of the single antenna.

Fig. 10 shows two cross bowtie antennas connected in series and both ends of the antenna are connected by using a 340 nm-long and 30 nm-wide metallic trace. In this case, a standing wave is formed on the trace and current nulls are maintained at the ends of the antennas; thus, the current distribution on the antennas is not affected. Fig. 11 also

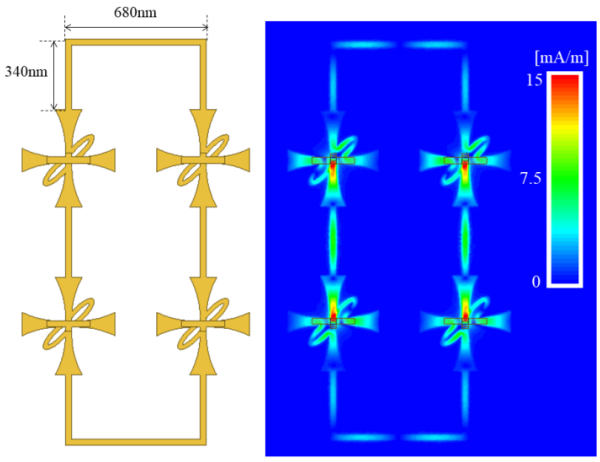

FIGURE 11. The geometry of the 2 × 2 cross bowtie antenna array and surface current distribution (tangential magnetic field) on the surface of the antennas with the vertically polarized wave illumination.

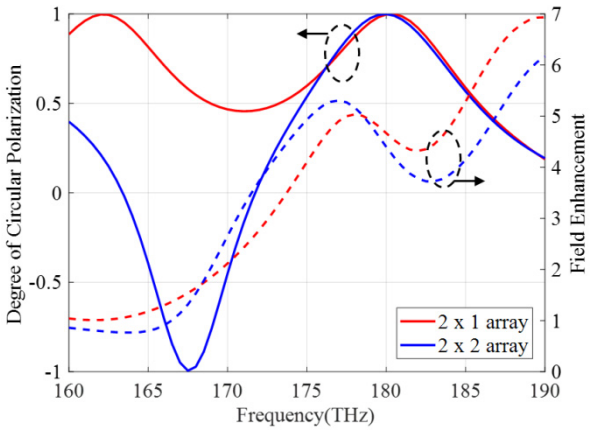

FIGURE 12. The degree of CP and the average field enhancement values in all the InGaAsSb loads from the optimized 2 × 1 and 2 × 2 cross-tapered bowtie antenna arrays.

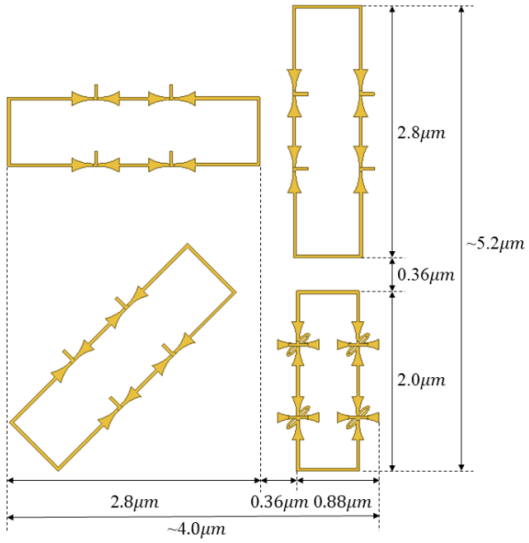

FIGURE 13. Illustration of a focal plane array for the full Stokes IR polarimeter using arrays of the vertical, horizontal, 45°-titled, and RHCP antennas.

shows a 2 × 2 cross bowtie antenna array where a pair of the antenna arrays from Fig. 10 is connected in parallel. The horizontal metallic traces for the parallel connection are tuned to 680 nm. This length also minimizes the current at the ends of the antennas and the corners of the metallic traces; thus, unnecessary radiation is reduced. After determining the lengths of the metallic traces, the antenna element itself has to be tuned slightly to maintain the unity degree of CP calculated from the near-fields in the load. This tuning is required because the metallic traces are also sensitive to the incident waves which are polarized along the traces. As a result, the 2 × 1 array with slightly shorter dimensions with L = 460 nm and W = 440 nm and the 2 × 2 array with the same L and W but with a shorter elliptical line whose major axis is 90 nm instead of 100 nm provide almost the perfect CP at 180 THz while maintaining field enhancement values near ∼4.5 for each antenna's load as shown in Fig. 12. For brevity, the averaged field enhancement values in all the InGaAsSb loads inside the antenna arrays are used. Lastly, it should be noted that an array of CP antennas of any number can be constructed using the lengths of the optimized metallic traces found from the 2 × 1 and 2 × 2 CP antenna arrays.

Finally, to be used as a polarimeter, a focal plane array based on the proposed antenna arrays is introduced. Previously, full Stokes polarimeters were realized using linear and circular polarizers combined with a polarization-blind sensor [3], [9], [11]–[15]. Here, a focal plane array using semiconductor-coupled antenna arrays for CP and linear polarization detection is proposed as a new type of a full Stokes polarimeter. Specifically, the array consists of vertical, horizontal and 45°-tilted bowtie antennas to obtain S_0, S_1, and S_2 of the Stokes vector and the CP bowtie antennas to obtain the other S_3. Fig. 13 shows an illustration of a focal plane array where four antenna elements for each polarization are configured as an array and four polarization-dependent antenna arrays are combined. Here, the linearly polarized antenna used in the focal plane array is from the structure in Fig. 1. Then, the antenna is loaded with the InGaAsSb block at the terminal and the open-ended transmission lines are used for the impedance matching. The similar array configuration for the linearly polarized bowtie antennas was reported previously [41].

Different from the existing full-Stokes polarimeters using external sensors, the proposed focal plane array can detect the polarization component of the incident wave directly by measuring the amount of current generated in the semiconductor loaded at each antenna. The metallic traces connected to the antennas of each array are used to collect DC current from each semiconductor load. From Fig. 13, it can be seen that the pixel size which represents the device size capable of measuring all the polarization components is within 4.0 μm × 5.2 μm by setting the distance between polarization-dependent arrays

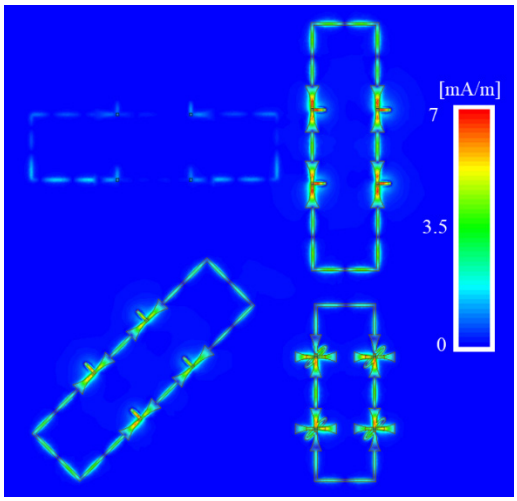

FIGURE 14. Surface current distribution (tangential magnetic field) on the surface of the focal plane array with the vertically polarized wave illumination.

to 360 nm. To verify the functionality of the focal plane array from Fig. 13, the surface current distribution on the surface of the array with a vertically polarized wave at normal incidence is calculated and shown in Fig. 14. From this calculation, we can observe that current nulls at the edges of the metallic traces are maintained and surface current of the four different arrays is properly distributed according to the polarization state of the incident wave, for example, high current values near the loads from the vertically polarized and the RHCP array, medium current levels from the 45°-tilted array, and negligible current levels from the horizontally polarized array. For low coupling among the array elements, the distance between arrays can be increased up to the half-wavelength (∼833 nm) of 180 THz. This condition leads to a dimension of the pixel within $6\,\mu\text{m} \times 6\,\mu\text{m}$ which is still smaller than a pixel size of $7.4\,\mu\text{m} \times 7.4\,\mu\text{m}$ from the full Stokes polarimeters using liquid crystal polymer-based micro-polarizers [3], [13], [14]. In addition, these conventional polarimeters require quarter-wave thick wave-plates, but the proposed antenna-based focal plane array requires only nanometer-sized semiconductor blocks. Due to the small size of the active material used in the antenna array, noise current can be reduced and the sensitivity of the polarimeter can also be improved. Therefore, a focal plane array based on the linearly polarized antennas and the proposed CP antennas capable of measuring the full Stokes vector of the IR incident wave can be used as a high-resolution and sensitive IR polarimeter.

V. CONCLUSION

In conclusion, we have presented a cross-tapered bowtie antenna composed of a vertical, a horizontal antenna, and two elliptical loops for CP detection in the IR spectrum. By connecting adjacent tips of the perpendicular antennas for a 90° phase shift, the loops realize a single terminal of the cross antenna where a detecting material can be mounted and thus the field enhancement from the antenna can be fully utilized. In full-wave simulations, a low-bandgap semiconductor, i.e., InGaAsSb, is mounted at the antenna terminal and the cross bowtie antenna is designed to absorb CP at the desired frequency (180 THz) where the maximum quantum efficiency of the InGaAsSb material is shown. The reactance of the InGaAsSb material which lowers the resonant frequency of the antenna is compensated for by using extra open-ended transmission lines connected to the terminal of the antenna. The final InGaAsSb-coupled CP antenna shows ∼6.5 of the field enhancement value and 25.88% of the absorption rate in the antenna terminal at 180 THz when a RHCP wave is incident; these values are higher than those for incident waves with different polarization states. This higher field enhancement and absorption of the antenna with the CP incident wave prove that the cross bowtie antenna coupled with the InGaAsSb can be utilized for a CP detector in the IR spectrum. Also, 2×1 and 2×2 arrays, where the CP cross bowtie antennas are connected with metallic traces, are designed and the numerical simulation shows that the unity degrees of CP from the arrays are maintained at 180 THz. As a focal plane array to be used for a full Stokes polarimeter, 2×2 arrays made up of the vertical, horizontal, 45°-tilted bowtie antennas, and the CP cross bowtie antennas are arranged with 360 nm distance and this array provides a pixel size near $4.0\,\mu\text{m} \times 5.2\,\mu\text{m}$. This pixel is smaller than a pixel ($7.4\,\mu\text{m} \times 7.4\,\mu\text{m}$) from the full Stokes polarimeters using the liquid crystal polymer-based micro-polarizers. Therefore, the proposed focal plane array based on the InGaAsSb-coupled CP antennas can be a viable solution for high-resolution and sensitive full Stokes IR polarimeter.

REFERENCES

[1] J. S. Tyo, D. L. Goldstein, D. B. Chenault, and J. A. Shaw, "Review of passive imaging polarimetry for remote sensing applications," *Appl. Opt.*, vol. 45, no. 22, pp. 5453–5469, 2006.
[2] G. C. Giakos, "Multifusion, multispectral, optical polarimetric imaging sensing principles," *IEEE Trans. Instrum. Meas.*, vol. 55, no. 5, pp. 1628–1633, Oct. 2006.
[3] W.-L. Hsu, J. Davis, K. Balakrishnan, M. Ibn-Elhaj, S. Kroto, N. Brock, and S. Pau, "Polarization microscope using a near infrared full-Stokes imaging polarimeter," *Opt. Express*, vol. 23, no. 4, pp. 4357–4368, Feb. 2015.
[4] J. Wang, W. Zheng, K. Lin, and Z. Huang, "Integrated Mueller-matrix near-infrared imaging and point-wise spectroscopy improves colonic cancer detection," *Biomed. Opt. Express*, vol. 7, no. 4, pp. 1116–1126, Apr. 2016.
[5] M. Garcia and V. Gruev, "Optical characterization of rigid endoscopes and polarization calibration methods," *Opt. Express*, vol. 25, no. 14, pp. 15713–15728, Jul. 2017.
[6] G. P. Nordin, J. T. Meier, P. C. Deguzman, and M. W. Jones, "Micropolarizer array for infrared imaging polarimetry," *J. Opt. Soc. Amer. A, Opt. Image Sci.*, vol. 16, no. 5, pp. 1168–1174, May 1999.
[7] V. Gruev, J. Van der Spiegel, and N. Engheta, "Dual-tier thin film polymer polarization imaging sensor," *Opt. Express*, vol. 18, no. 18, pp. 19292–19303, Aug. 2010.
[8] V. Gruev, R. Perkins, and T. York, "CCD polarization imaging sensor with aluminum nanowire optical filters," *Opt. Express*, vol. 18, no. 18, pp. 19087–19094, 2010.
[9] A. G. Andreou and Z. K. Kalayjian, "Polarization imaging: Principles and integrated polarimeters," *IEEE Sensors J.*, vol. 2, no. 6, pp. 566–576, Dec. 2002.

[10] K. A. Bachman, J. J. Peltzer, P. D. Flammer, T. E. Furtak, R. T. Collins, and R. E. Hollingsworth, "Spiral plasmonic nanoantennas as circular polarization transmission filters," *Opt. Express*, vol. 20, no. 2, pp. 1308–1319, Jan. 2012.

[11] G. Myhre and S. Pau, "Imaging capability of patterned liquid crystals," *Appl. Opt.*, vol. 48, no. 32, pp. 6152–6158, Nov. 2009.

[12] X. Zhao, A. Bermak, F. Boussaid, and V. G. Chigrinov, "Liquid-crystal micropolarimeter array for full Stokes polarization imaging in visible spectrum," *Opt. Express*, vol. 18, no. 17, pp. 17776–17787, Aug. 2010.

[13] G. Myhre, W.-L. Hsu, A. Peinado, C. LaCasse, N. Brock, R. A. Chipman, and S. Pau, "Liquid crystal polymer full-stokes division of focal plane polarimeter," *Opt. Express*, vol. 20, no. 25, pp. 27393–27409, Dec. 2012.

[14] W.-L. Hsu, G. Myhre, K. Balakrishnan, N. Brock, M. Ibn-Elhaj, and S. Pau, "Full-Stokes imaging polarimeter using an array of elliptical polarizer," *Opt. Express*, vol. 22, no. 3, pp. 3063–3074, Feb. 2014.

[15] X. Zhao, X. Pan, X. Fan, P. Xu, A. Bermak, and V. G. Chigrinov, "Patterned dual-layer achromatic micro-quarter-wave-retarder array for active polarization imaging," *Opt. Express*, vol. 22, no. 7, pp. 8024–8034, Apr. 2014.

[16] J. J. Peltzer, K. A. Bachman, J. W. Rose, P. D. Flammer, T. E. Furtak, R. T. Collins, and R. E. Hollingsworth, "Plasmonic micropolarizers for full Stokes vector imaging," *Proc. SPIE*, vol. 8364, Jun. 2012, Art. no. 83640O.

[17] B. Päivänranta, N. Passilly, J. Pietarinen, P. Laakkonen, M. Kuittinen, and J. Tervo, "Low-cost fabrication of form-birefringent quarter-wave plates," *Opt. Express*, vol. 16, no. 21, pp. 16334–16342, Oct. 2008.

[18] Y. Pang and R. Gordon, "Metal nano-grid reflective wave plate," *Opt. Express*, vol. 17, no. 4, pp. 2871–2879, Feb. 2009.

[19] S.-Y. Hsu, K.-L. Lee, E.-H. Lin, M.-C. Lee, and P.-K. Wei, "Giant birefringence induced by plasmonic nanoslit arrays," *Appl. Phys. Lett.*, vol. 95, no. 1, Jul. 2009, Art. no. 013105.

[20] M. R. Shcherbakov, M. I. Dobynde, T. V. Dolgova, D.-P. Tsai, and A. A. Fedyanin, "Full Poincaré sphere coverage with plasmonic nanoslit metamaterials at Fano resonance," *Phys. Rev. B, Condens. Matter*, vol. 82, no. 19, Nov. 2010, Art. no. 193402.

[21] A. Drezet, C. Genet, and T. W. Ebbesen, "Miniature plasmonic wave plates," *Phys. Rev. Lett.*, vol. 101, no. 4, Jul. 2008, Art. no. 043902.

[22] Y. Gorodetski, E. Lombard, A. Drezet, C. Genet, and T. W. Ebbesen, "A perfect plasmonic quarter-wave plate," *Appl. Phys. Lett.*, vol. 101, no. 20, Nov. 2012, Art. no. 201103.

[23] P. Biagioni, J. S. Huang, L. DuÃš, M. Finazzi, and B. Hecht, "Cross Resonant Optical Antenna," *Appl. Phys. Lett.*, vol. 102, no. 25, p. 256801, Jun. 2009.

[24] P. Biagioni, M. Savoini, J.-S. Huang, L. Duò, M. Finazzi, and B. Hecht, "Near-field polarization shaping by a near-resonant plasmonic cross antenna," *Phys. Rev. B, Condens. Matter*, vol. 80, no. 15, Oct. 2009, Art. no. 153409.

[25] P. Klaer, G. Razinskas, M. Lehr, K. Krewer, F. Schertz, X.-F. Wu, B. Hecht, G. Schönhense, and H. J. Elmers, "Robustness of plasmonic angular momentum confinement in cross resonant optical antennas," *Appl. Phys. Lett.*, vol. 106, no. 26, Jun. 2015, Art. no. 261101.

[26] P. Klaer, G. Razinskas, M. Lehr, X. Wu, B. Hecht, F. Schertz, H.-J. Butt, G. Schönhense, and H. J. Elmers, "Polarization dependence of plasmonic near-field enhanced photoemission from cross antennas," *Appl. Phys. B*, vol. 122, no. 5, p. 136, May 2016.

[27] B. Abasahl, S. Dutta-Gupta, C. Santschi, and O. J. F. Martin, "Coupling strength can control the polarization twist of a plasmonic antenna," *Nano Lett.*, vol. 13, no. 9, pp. 4575–4579, Sep. 2013.

[28] N. Yu, F. Aieta, P. Genevet, M. A. Kats, Z. Gaburro, and F. Capasso, "A broadband, background-free quarter-wave plate based on plasmonic metasurfaces," *Nano Lett.*, vol. 12, no. 12, pp. 6328–6333, 2012.

[29] B. Yang, W.-M. Ye, X.-D. Yuan, Z.-H. Zhu, and C. Zeng, "Design of ultrathin plasmonic quarter-wave plate based on period coupling," *Opt. Lett.*, vol. 38, no. 5, pp. 679–681, Mar. 2013.

[30] H. Zhao, Y. Yang, Q. Li, and M. Qiu, "Sub-wavelength quarter-wave plate based on plasmonic patch antennas," *Appl. Phys. Lett.*, vol. 103, no. 26, Dec. 2013, Art. no. 261108.

[31] A. Roberts and L. Lin, "Plasmonic quarter-wave plate," *Opt. Lett.*, vol. 37, no. 11, pp. 1820–1822, Jun. 2012.

[32] F. J. González and G. D. Boreman, "Comparison of dipole, bowtie, spiral and log-periodic IR antennas," *Infr. Phys. Technol.*, vol. 46, no. 5, pp. 418–428, Jun. 2005.

[33] F. J. Gonzalez, B. Ilic, J. Alda, and G. D. Boreman, "Antenna-coupled infrared detectors for imaging applications," *IEEE J. Sel. Topics Quantum Electron.*, vol. 11, no. 1, pp. 117–120, Jan. 2005.

[34] L. Tang, S. E. Kocabas, S. Latif, A. K. Okyay, D.-S. Ly-Gagnon, K. C. Saraswat, and D. A. B. Miller, "Nanometre-scale germanium photodetector enhanced by a near-infrared dipole antenna," *Nature Photon.*, vol. 2, no. 4, pp. 226–229, Mar. 2008.

[35] M. W. Knight, H. Sobhani, P. Nordlander, and N. J. Halas, "Photodetection with active optical antennas," *Science*, vol. 332, no. 6030, pp. 702–704, 2011.

[36] J. A. Bean, A. Weeks, and G. D. Boreman, "Performance optimization of antenna-coupled Al/AlO_x/Pt tunnel diode infrared detectors," *IEEE J. Quantum Electron.*, vol. 47, no. 1, pp. 126–135, Jan. 2011.

[37] M. N. Gadalla, M. Abdel-Rahman, and A. Shamim, "Design, optimization and fabrication of a 28.3 THz nano-rectenna for infrared detection and rectification," *Sci. Rep.*, vol. 4, p. 4270, Mar. 2014.

[38] A. Alù and N. Engheta, "Input impedance, nanocircuit loading, and radiation tuning of optical nanoantennas," *Phys. Rev. Lett.*, vol. 101, no. 4, pp. 043901-1–043901-4, Jul. 2008.

[39] Y. Xu, E. Tucker, G. Boreman, M. B. Raschke, and B. A. Lail, "Optical nanoantenna input impedance," *ACS Photon.*, vol. 3, no. 5, pp. 881–885, May 2016.

[40] C. J. Vineis, "Characterization of OMVPE-grown GaSb-based epilayers using in situ reflectance and ex situ TEM," M.S. thesis, Dept. Mater. Sci. Eng., Massachusetts Inst. Technol., Cambridge, MA, USA, 2001.

[41] K. Sarabandi and S. Choi, "Design optimization of bowtie nanoantenna for high-efficiency thermophotovoltaics," *J. Appl. Phys.*, vol. 114, no. 21, Dec. 2013, Art. no. 214303.

[42] M. S. Eggleston, K. Messer, L. Zhang, E. Yablonovitch, and M. C. Wu, "Optical antenna enhanced spontaneous emission," *Proc. Nat. Acad. Sci. USA*, vol. 112, no. 6, pp. 1704–1709, 2015.

[43] M. Walther, D. G. Cooke, C. Sherstan, M. Hajar, M. R. Freeman, and F. A. Hegmann, "Terahertz conductivity of thin gold films at the metal-insulator percolation transition," *Phys. Rev. B, Condens. Matter*, vol. 76, no. 12, Sep. 2007, Art. no. 125408.

[44] P. M. Krenz, B. Tiwari, G. P. Szakmany, A. O. Orlov, F. J. González, G. D. Boreman, and W. Porod, "Response increase of IR antenna-coupled thermocouple using impedance matching," *IEEE J. Quantum Electron.*, vol. 48, no. 5, pp. 659–664, May 2012.

[45] S. Choi, "Cross bowtie antenna-coupled detector for circularly polarized infrared wave sensing," in *Proc. Int. Symp. Antennas Propag. (ISAP)*, Oct. 2018, pp. 1–2.

[46] S. Choi and K. Sarabandi, "A W-shaped antenna with spatial polarization variation for direction finding," *IEEE Antennas Wireless Propag. Lett.*, vol. 17, no. 12, pp. 2429–2433, Dec. 2018.

[47] M. Silva-López, A. Cuadrado, N. Llombart, and J. Alda, "Antenna array connections for efficient performance of distributed microbolometers in the IR," *Opt. Express*, vol. 21, no. 9, pp. 10867–10877, May 2013.

SANGJO CHOI (S'10–M'17) received the B.S. degree in electronic engineering from Kyungpook National University, Daegu, South Korea, the B.S. degree in electrical engineering from The University of Texas at Dallas, Dallas, TX, USA, in 2008, and the M.S. and Ph.D. degrees in electrical engineering from The University of Michigan at Ann Arbor, Ann Arbor, MI, USA, in 2010 and 2014, respectively.

He was a Senior Engineer with Qualcomm, Inc., San Diego, CA, USA, from 2014 to 2017. Since 2017, he has been an Assistant Professor in electrical engineering from the University of Ulsan, Ulsan, South Korea. He holds three U.S. patents. His current research interests include antennas for infrared detectors and energy harvesting devices, plasmonics, metasurfaces, band-gap structures, RF packages and modules for wireless communication.

Dr. Choi received the Kwanjeong Scholarship from Kwanjeong Education Foundation, South Korea, in 2008. He was a recipient of the Honorable Mention and one of the Finalists from the IEEE International Symposium on Antenna and Propagation Student Paper Competition, in 2010 and 2013.

KAMAL SARABANDI (S'87–M'90–SM'92–F'00) received the B.S. degree in electrical engineering from the Sharif University of Technology, Tehran, Iran, in 1980, the M.S. degree in electrical engineering from The University of Michigan at Ann Arbor, Ann Arbor, MI, USA, in 1986, and the M.S. degree in mathematics and the Ph.D. degree in electrical engineering from The University of Michigan, in 1989.

He led the Center for Microelectronics and Sensors sponsored by the Army Research Laboratory under the Micro-Autonomous Systems and Technology (MAST) Collaborative Technology Alliance (CTA) Program, from 2008 to 2018. He is currently the Director of the Radiation Laboratory and the Rufus S. Teesdale endowed Professor of engineering with the Department of Electrical Engineering and Computer Science, The University of Michigan at Ann Arbor. He is also leading a newly established center in Microwave Sensor Technology funded by the King Abdulaziz City for Science and Technology (KACST). He leads a large research group including two research scientists and 16 Ph.D. students and two postdoctoral fellows. He has graduated 51 Ph.D. and supervised numerous postdoctoral students. He has published many book chapters and more than 290 articles in refereed journals on miniaturized and on-chip antennas, meta-materials, electromagnetic scattering, wireless channel modeling, random media modeling, microwave measurement techniques, radar calibration, inverse scattering problems, and microwave sensors. He has also had more than 690 articles and invited presentations in many national and international conferences and symposia on similar subjects. Over the past 30 years, his research has been focused on applied electromagnetics and has made significant contributions to science and technology of microwave and millimeter-wave radar remote sensing, antennas, communication channel modeling, microwave sensors, and radar systems. He has served as the Principal Investigator for many projects sponsored by the National Aeronautics and Space Administration (NASA), Jet Propulsion Laboratory (JPL), Army Research Office (ARO), Office of Naval Research (ONR), Army Research Laboratory (ARL), National Science Foundation (NSF), Defense Advanced Research Projects Agency (DARPA), and a large number of industries. His research interests include microwave and millimeter-wave radar remote sensing, meta-materials, electromagnetic wave propagation, and antenna miniaturization.

Dr. Sarabandi served as a member for the NASA Advisory Council appointed by the NASA Administrator for two consecutives from 2006 to 2010. He was a member of the Editorial Board of the PROCEEDINGS OF THE IEEE. He was selected as a Fellow of the American Association for the Advancement of Science (AAAS). He is a member of Commissions F and B of URSI. He was a recipient of the Henry Russel Award from the Regent of The University of Michigan, in 1997. In 1999, he was also a recipient of the GAAC Distinguished Lecturer Award from the German Federal Ministry for Education, Science, and Technology, the 1996 EECS Department Teaching Excellence Award, the IEEE GRSS Distinguished Achievement Award, in 2005, the University of Michigan Faculty Recognition Award, the Best Paper Award at the 2006 Army Science Conference, and the IEEE GRSS Symposium Best Paper Award, in 2008 and 2017, the Humboldt Research Award from The Alexander von Humboldt Foundation of Germany, in 2008, and the 2010 Distinguished Faculty Achievement Award from The University of Michigan. The IEEE Board of Directors announced him as a recipient of the 2011 IEEE Judith A. Resnik Award. He was recognized by the IEEE GRSS with its 2013 Education Award. He was a recipient of the Research Excellence Award, in 2004, the Stephen S. Attwood Award, in 2017, and the Ted Kennedy Family Faculty Team Excellence Award, in 2018, from the College of Engineering, The University of Michigan. He was also a recipient of the NASA Group Achievement Award for his contributions to NASA SMAP mission. In the past several years, joint papers presented by his students at a number of international symposia (IEEE APS'95,'97,'00,'01,'03,'05,'06,'07;'16;'19, IEEE IGARSS'99,'02,'07;'11,'14, IEEE IMS'01, USNC URSI'04,'05,'06,'10,'11, AMTA'06, URSI GA '08,'14; Eastern Snow Conference'16, and IEEE MTT-NEMO'19) have received best paper awards. He is serving as the Chair for the USNC URSI Commission F. He was an Associate Editor of the IEEE TRANSACTIONS ON ANTENNAS AND PROPAGATION and the IEEE SENSORS JOURNAL. He served as the President for the IEEE Geoscience and Remote Sensing Society (GRSS), in 2015 and 2016. In 2016, he has been recognized as one of the top 50 graduates of the Sharif University of Technology since its establishment.